Brain-specific deletion of neuropathy target esterase/*swisscheese* results in neurodegeneration

Katerina Akassoglou*†, Brian Malester*‡, Jixiang Xu*, Lino Tessarollo§, Jack Rosenbluth‡¶, and Moses V. Chao*‡‖**

*Molecular Neurobiology Program, Skirball Institute of Biomolecular Medicine, Departments of ‖Cell Biology and ‡Physiology and Neuroscience, and ¶Rusk Institute, RR7714, New York University School of Medicine, New York, NY 10016; †Department of Pharmacology, University of California at San Diego, La Jolla, CA 92093-0636; and §Neural Development Group, Mouse Cancer Genetics Program, National Cancer Institute, Frederick, MD 21701

Communicated by Thomas S. Reese, National Institutes of Health, Bethesda, MD, February 12, 2004 (received for review September 16, 2003)

Neuropathy target esterase (NTE) is a neuronal membrane protein originally identified for its property to be modified by organophosphates (OPs), which in humans cause neuropathy characterized by axonal degeneration. *Drosophila* mutants for the homolog gene of *NTE*, *swisscheese* (*sws*), indicated a possible involvement of *sws* in the regulation of axon–glial cell interaction during glial wrapping. However, the role of NTE/*sws* in mammalian brain pathophysiology remains unknown. To investigate NTE function *in vivo*, we used the cre/loxP site-specific recombination strategy to generate mice with a specific deletion of NTE in neuronal tissues. Here we show that loss of NTE leads to prominent neuronal pathology in the hippocampus and thalamus and also defects in the cerebellum. Absence of NTE resulted in disruption of the endoplasmic reticulum, vacuolation of nerve cell bodies, and abnormal reticular aggregates. Thus, these results identify a physiological role for NTE in the nervous system and indicate that a loss-of-function mechanism may contribute to neurodegenerative diseases characterized by vacuolation and neuronal loss.

cre/lox P | vacuolation | thalamus | hippocampus | Purkinje cells

Neuropathy target esterase (NTE) is a 150-kDa transmembrane protein that is highly conserved among species including insects, nematodes, yeast, and bacteria (1). Mutations in the *Drosophila* homolog, *swisscheese* (*sws*), produced glial-axonal hyperwrapping, degeneration, and a shortened life span (2). Both neurons and glia underwent cell death, accompanied by extensive vacuolation in the nervous system of *Drosophila sws* mutants. The NTE protein represents the mammalian homolog of the *Drosophila swisscheese* gene (3). The *swisscheese* and NTE proteins share a number of motifs including several hydrophobic transmembrane sequences, a serine esterase domain, and a sequence similar to the regulatory subunit of protein kinase A. A variety of pharmacological experiments have established the involvement of NTE in organophosphate (OP)-induced delayed neuropathy in humans and in animal models (3, 4), presumably through inactivation of the serine esterase activity. The protein NTE was initially identified as a target of OPs, found in pesticides and chemical warfare agents that cause peripheral neuropathy in humans (5, 6). OP-induced neuropathy has been implicated in Gulf War disease and other toxic neuropathies. However, the physiological functions of NTE, as well as the downstream events of NTE-induced neuropathy after OP exposure, remain unknown.

We therefore sought to examine the physiological role of NTE in the central nervous system. Knockout of the *NTE* gene is embryonic lethal in mice at an early embryonic age (4, 19), thereby precluding the study of the role of NTE in the adult brain. We therefore constructed a conditional mutant *NTE* strain and deleted NTE specifically in neuronal tissues. We show here that neuron-specific deletion of NTE causes vacuolation of neuronal bodies and dendrites. The NTE protein was found to associate with the endoplasmic reticulum (ER) of hippocampal neurons. Interestingly, vacuolar pathology in the hippocampus and thalamus of NTE-depleted mice was closely associated with ER breakdown. Taken together, our results demonstrate that inhibition of NTE function leads to disruption of the ER and vacuolar pathology in the nervous system.

Methods

Generation of NTE Conditional Mice. Genomic NTE DNA was cloned from a SVJ129 mouse genomic phage library by using human NTE mRNA sequence AJ004832 as a probe. The targeting construct introduced a *loxP* site in the intron preceding exon 6 and a floxed *neomycin* resistance cassette in the 5′ untranslated region. The *neomycin* cassette was removed subsequently from targeted ES cell clones by transient expression of Cre, yielding the final floxed locus. Three separate ES clones (BB10, CF4, and GG8) were injected into blastocysts and implanted into pseudopregnant mothers to generate chimeras. $NTE^{flox/+}$ mice were generated from all three clones and were crossed to Nes-cre mice. Nes-cre:$NTE^{fl/+}$ mice were crossed to $NTE^{fl/+}$ mice to generate Nes-cre:$NTE^{fl/fl}$ mice as well as $NTE^{fl/fl}$ and $NTE^{+/+}$ littermate control mice. A PCR assay was used to genotype tail DNA by using NTE sense 5′-GCTTAAGGGCACCTGCCAGC-3′ and NTE antisense primer 5′-GGTCTTGTAGCCTGCAGTCC-3′ that amplify a 346-bp fragment in WT animals and an additional 110 bp for the loxP site in conditionally targeted animals. Nes-cre mice were genotyped by using a sense 5′-GCGGTCTGGCAGTAAAAACTATC-3′ and an antisense primer that amplify 100 bp of the cre gene.

Immunoblot. Brains from $NTE^{fl/fl}$ and Nes-cre:$NTE^{fl/fl}$ mice were homogenized in lysis buffer, and equal amounts of protein were loaded on a 4–16% gradient SDS/PAGE gel and transferred to poly(vinylidene difluoride) (PVDF) membranes (Millipore, Bedford, MA). Primary antibodies used were rabbit polyclonal antibody generated against amino acids 798-1231 of NTE (R979, 1/1,000), mouse anti-GM130 (1/250, Transduction Laboratories, Lexington, KY), rabbit anti-ribophorin (from Gert Kreibich, 1/1,000). Secondary antibodies include anti-rabbit horseradish peroxidase (HRP) (Cell Signaling, Beverly, MA, 1/10,000), protein-A-HRP (Zymed, South San Francisco, CA, 1/7,500), and anti-mouse-HRP (Sigma, 1/10,000). Control membranes were stripped and reprobed with an antibody against GAPDH (Novus, Littleton, CO, 1/2,000) or β-actin (Sigma, 1/5,000). Detection of HRP used chemiluminescence (Amersham UK).

Esterase Assays. NTE and acetylcholine esterase (AChE) assays were performed exactly as described (4). Mipafox and phenyl valerate were purchased from Polycarbon Industries, Devens, MA; paraoxon, aminoantipyrine, potassium ferricyanide, acetylthiocholine, and 5,5′-dithio-bis-2-nitrobenzoic acid were purchased from Sigma. NTE activity is expressed as percentage of

Abbreviations: AChE, acetylcholine esterase; ER, endoplasmic reticulum; OP, organophosphate; NTE, neuropathy target esterase; E*n*, embryonic day *n*.

**To whom correspondence should be addressed. E-mail: chao@saturn.med.nyu.edu.

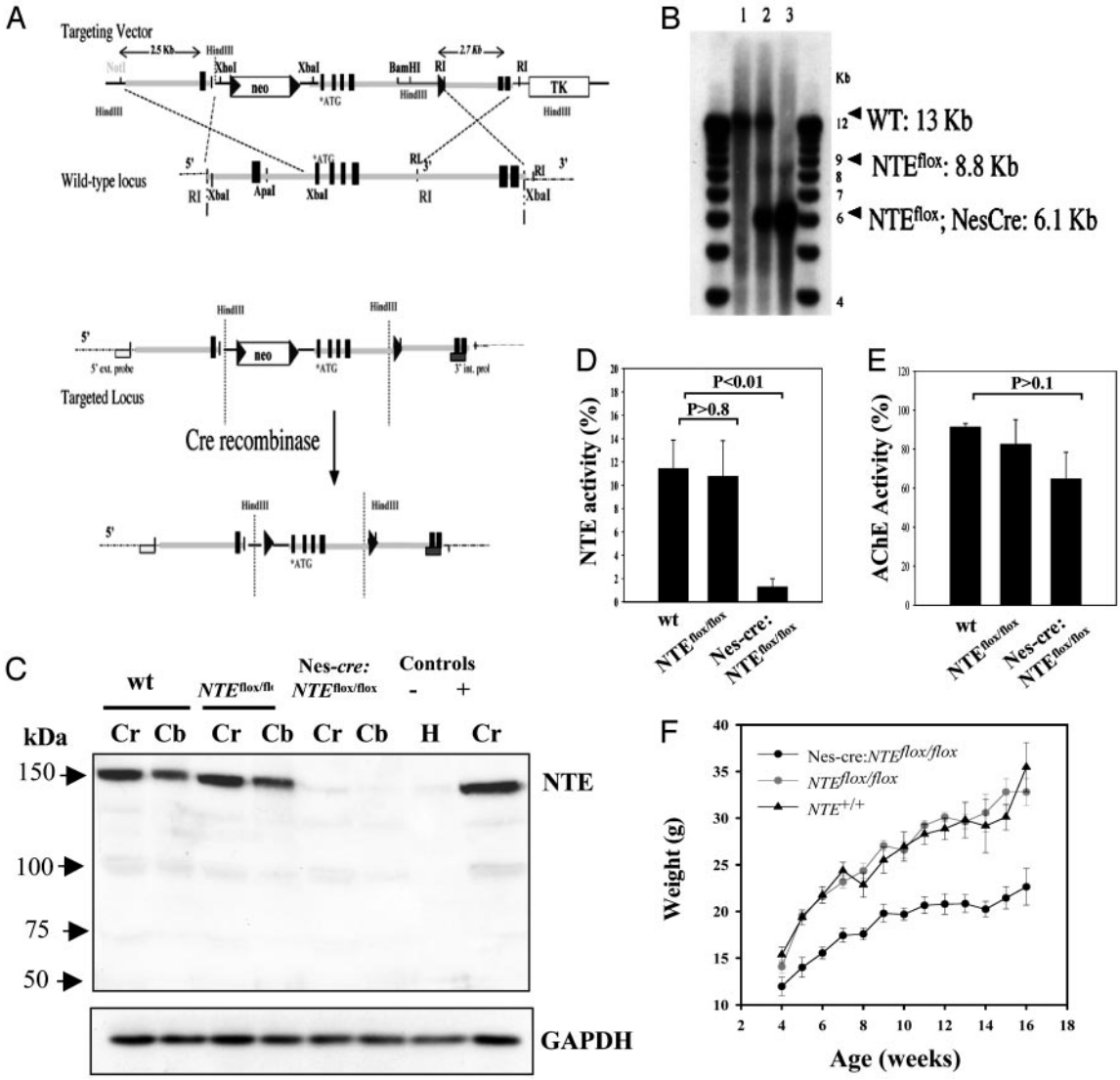

Fig. 1. Brain specific inactivation of the NTE gene. (*A*) Diagram of targeting construct and strategy. Exons are indicated as black boxes. Gray box, 3′ internal probe; box, 3′ external probe; triangles, LoxP sites. (*B*) Genomic Southern blot from WT (lane 1), Nes-cre:$NTE^{fl/+}$ (lane 2), and Nes-cre:$NTE^{fl/fl}$ (lane 3). Brain DNA was cleaved with *Spe*I and hybridized with a ^{32}P- labeled 5′ external probe. (*C*) NTE is missing from the brains of Nes-cre:$NTE^{fl/fl}$ mice. Immunoblot analysis using an antibody against NTE from brain extracts of the cerebrum (Cr) and cerebellum (Cb) from WT, $NTE^{fl/fl}$, and Nes-cre:$NTE^{fl/fl}$ mice. Heart (H) and cerebrum (Cr) were used as negative (−) and positive (+) controls, respectively. Immunoblot using an antibody against GAPDH was used to ensure equal loading between samples. (*D*) Nes-cre:$NTE^{fl/fl}$ mice (1.26 ± 0.72%, $n = 5$) had ≈90% less NTE activity in the brain ($P < 0.01$), when compared to WT mice (11.41 ± 2.47%, $n = 5$). $NTE^{fl/fl}$ mice (10.75 ± 3.06%, $n = 5$) showed no difference when compared to WT control mice. (*E*) No statistically significant differences were observed for AChE activity. (*F*) Weight curve of Nes-cre:$NTE^{fl/fl}$ mice ($n = 16$), $NTE^{fl/fl}$ ($n = 14$) and $NTE^{+/+}$ ($n = 9$) littermate controls. There is no difference between $NTE^{fl/fl}$ and $NTE^{+/+}$ mice, whereas Nes-cre:$NTE^{fl/fl}$ weighed less after 5 weeks of age ($P < 0.0001$).

total phenyl valerate-hydrolyzing activity. AChE activity is expressed as a percentage of WT brain activity.

Immunohistochemistry. Silver staining and immunohistochemical staining was performed on cryostat sections (7). Primary antibodies were goat anti-human calbindin (1:4,000; Sigma); anti-human mitogen-activated protein (MAP)-2 (1:400; Chemicon, Temecula, CA). Nissl staining using Texas red fluorescent Nissl (Molecular Probes,) was performed according to instructions. For immunocytochemistry, primary hippocampal neurons were fixed in a 1:1 solution of ethanol/methanol followed by acetone permeabilization at 4°C. Rabbit anti-NTE (R979), mouse anti-calnexin (Chemicon), anti-rabbit-Cy3, and anti-mouse-FITC (The Jackson Laboratories) were used at 1:200. Confocal images (Bio-Rad) were analyzed with IMAGE J software.

EM Analysis. Mice were anesthetized with pentobarbital and fixed by transcardiac perfusion with 3% glutaraldehyde/2% formaldehyde in cacodylate buffer (pH 7.3). Brain and spinal cord were dissected and 1- to 2-mm-thick coronal or sagital slices were rinsed, postfixed in 2% osmium tetroxide/ferricyanide in cacodylate buffer, dehydrated through methanol and propylene oxide, and embedded in Araldite. Sections (1 μm) were stained with toluidine blue and further sections (0.1 μm) were stained with potassium permanganate and uranyl acetate and examined in a Phillips EM300 microscope.

Cell Culture and Subcellular Fractionation. Hippocampal neurons were obtained from E18 rats as described (8). Primary neurons (DIV 11) were homogenized and subjected to Optiprep gradient centrifugation (8). Membrane fractions were collected and analyzed by immunoblotting.

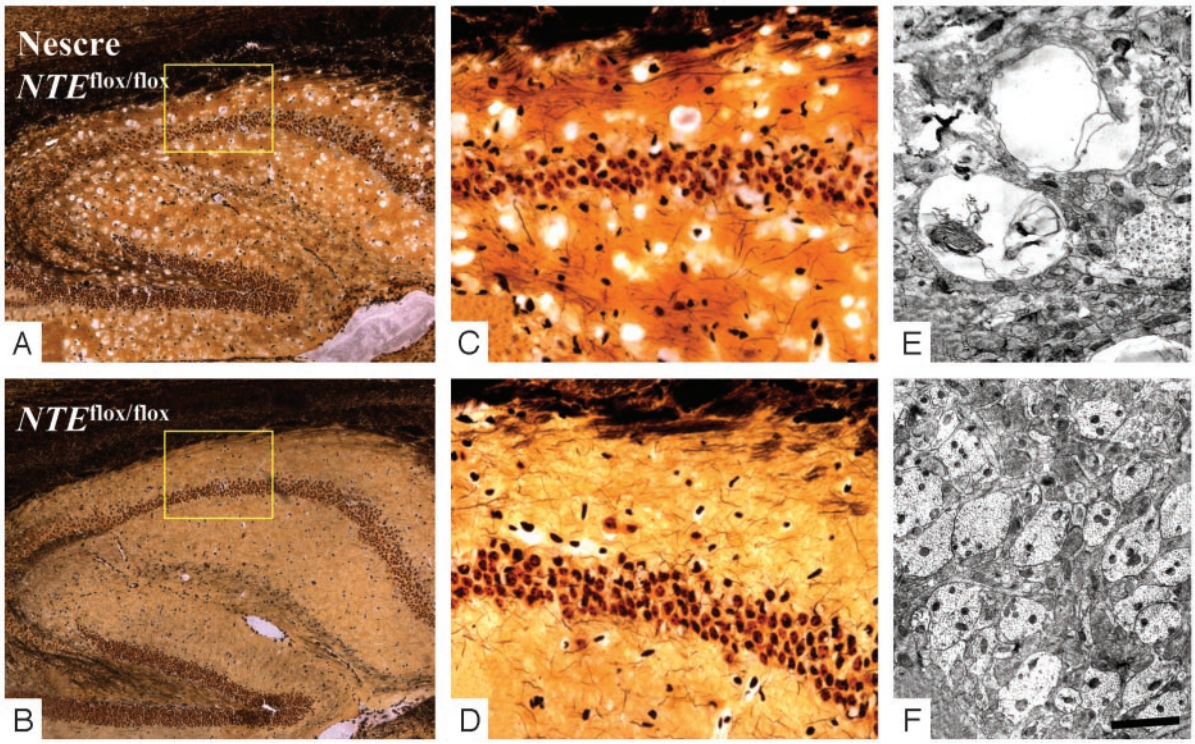

Fig. 2. Deletion of NTE induces hippocampal vacuolation. (*A*) Extensive vacuolation in the neuropil of the hippocampus of Nes-cre:$NTE^{fl/fl}$. (*B*) Normal hippocampal morphology of $NTE^{fl/fl}$ littermate control. Boxes are enlarged in *C* and *D*. (*C*) Vacuolation in the CA2 neuropil area of Nes-cre:$NTE^{fl/fl}$. (*D*) Normal CA2 neuropil of $NTE^{fl/fl}$ mice. (*E*) Hippocampal neuropil of Nes-cre:$NTE^{fl/fl}$ mice contained swollen dendrites with large vacuoles and abnormal membranous inclusions. (*F*) Normal appearance of 4.5-month-old $NTE^{fl/fl}$ hippocampal neuropil. (Scale bar, 250 μm in *A* and *B*; 36 μm in *C* and *D*; 1 μm in *E*; and 4.5 μm in *F*.)

Rotarod Behavior Test. The rotarod assay was performed on a TSE RotaRod apparatus purchased from TSE Technical and Scientific Equipment GmbH. The rod was turning at a speed constant of 20 revolutions per min. Rotarod assays were conducted for five consecutive days with a 300-s maximal time limit. Means were collected for at least three trials per day. Statistical calculations were made by using Student's *t* test.

Results

Brain-Specific Inactivation of the NTE Gene. NTE is an integral membrane protein, expressed predominantly by neurons in the brain starting at early embryonic development (9, 10). Because inactivation of the mouse *NTE* gene is lethal at an early embryonic age (ref. 4 and J.X., unpublished data), we constructed a conditional mutant *NTE* strain ($NTE^{fl/fl}$; Fig. 1 *A* and *B*). To inactivate the *NTE* gene in the adult brain, we bred the $NTE^{fl/fl}$ strain with Nestin-cre (Nes-cre) mice, which express cre recombinase after E11 in the central and peripheral nervous system (11) (Fig. 1*B*). Nes-cre:$NTE^{fl/fl}$ mice are born in normal ratios, showing that deletion of NTE after E11 is compatible with embryonic CNS development.

Western blot analysis using a rabbit polyclonal antibody against NTE showed that NTE was not detected in the brain of Nes-cre:$NTE^{fl/fl}$ mice (Fig. 1*C*). Examination of NTE esterase activity in brain homogenates of Nes-cre:$NTE^{fl/fl}$ mice indicated that the Nes-cre transgene abolished 90% of NTE activity (Fig. 1*D*). An AChE assay performed as a control did not show a significant reduction between Nes-cre:$NTE^{fl/fl}$ and WT mice (Fig. 1*E*). Phenotypic abnormalities of Nes-cre:$NTE^{fl/fl}$ mice include abnormal flexion reflex by 4 weeks of age and reduced weight gain (Fig. 1*F*) when compared to $NTE^{fl/fl}$ controls.

Hippocampal and Thalamic Vacuolation. At 2 weeks of age, the brain structure of Nes-cre:$NTE^{fl/fl}$ mice appeared normal, without any pathological signs. At six weeks of age, the conditional NTE mice developed prominent hippocampal pathology. Silver staining of Nes-cre:$NTE^{fl/fl}$ mice revealed extensive vacuolation in CA1, CA2, and CA3 regions, as well as the polymorphic area of the dentate gyrus (Fig. 2*A*), when compared to $NTE^{fl/fl}$ littermate (Fig. 2*B*). High-magnification images of the hippocampus of the Nes-cre:$NTE^{fl/fl}$ mice revealed specific vacuolation at the neuropil (Fig. 2*C*) when compared to $NTE^{fl/fl}$ littermate controls (Fig. 2*D*). The morphology of the cell body layer was unaffected. No evidence of apoptosis was observed by terminal deoxynucleotidyltransferase-mediated dUTP nick end labeling (TUNEL) or assay of activated caspases (data not shown).

To further characterize vacuolation in the neuropil, electron microscopic (EM) analysis was carried out. Large vacuoles and abnormal membranous folds within dendritic processes of the hippocampal neurons were observed (Fig. 2*E*). In contrast, the neuropil of the $NTE^{fl/fl}$ mice displayed normal dendritic morphology (Fig. 2*F*). Prominent vacuolation was also observed in thalamic neurons beginning at six weeks of age (Fig. 3*H*). Silver staining at 3 months of age showed extensive loss of large thalamic neurons in the Nes-cre:$NTE^{fl/fl}$ mice (Fig. 3*A*), when compared to littermate $NTE^{fl/fl}$ controls (Fig. 3*C*). Confocal microscopy revealed vacuolation and a dramatic redistribution of rough ER (Fig. 3 *B* and *E–G*), as assayed by fluorescent Nissl staining in neurons of Nes-cre:$NTE^{fl/fl}$ mice, when compared to $NTE^{fl/fl}$ controls (Fig. 3*D*).

ER Localization. What is the cellular basis for these observations? Previous experiments in monkey kidney COS7 cells demonstrated that GFP-tagged NTE colocalized with calnexin, an ER marker (11). However, the subcellular localization of NTE in neurons is unknown. To determine the subcellular localization of NTE in neurons, we established primary cultures of hippocampal

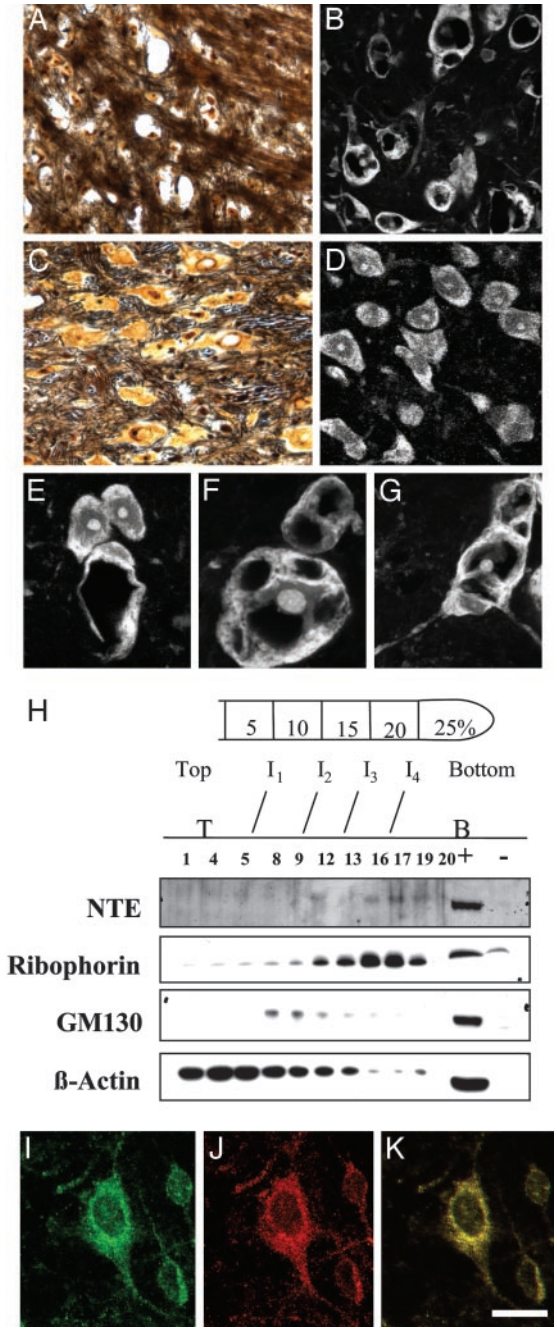

Fig. 3. NTE localizes to the ER and its deletion results in redistribution of Nissl substance in the thalamic neurons. (*A* and *B*) Silver staining showing neuronal loss in the thalamus of a Nes-cre:$NTE^{fl/fl}$ mice mouse (3 months) (*A*) when compared to age-matched $NTE^{fl/fl}$ mouse (*C*). (*E*, *F*, and *G*) Fluorescent Nissl stain showing vacuolated neurons in Nes-cre:$NTE^{fl/fl}$ mice. (*D*) Normal distribution of Nissl substance in the cell body of $NTE^{fl/fl}$ mice. (*E*) Six-week-old Nes-cre:$NTE^{fl/fl}$ mouse at the onset of neuronal pathology showing two normal and one vacuolated neuron. (*H*) Subcellular fractionation of hippocampal neurons shows the presence of NTE in the ribophorin, ER-containing fraction, and not in the GM130, Golgi-containing fraction. +, positive control, cerebrum lysate; −, negative control, heart lysate; I, interface between gradients; T, top of gradient; B, bottom of gradient. Double immunofluorescence for calnexin (*J*) and NTE (*I*) in primary hippocampal neurons shows association of NTE with the ER (*K*). (Scale bar, 36 μm in *A–C*; 25 μm in *B–D*; and 13 μm in *E–G*.)

neurons and performed subcellular fractionation. When we used ribophorin as a specific ER marker and GM130 as a specific Golgi marker, we observed that NTE was present at the ribophorin-positive fractions (Fig. 3*H*). In addition, double immunofluorescence for the ER marker calnexin (Fig. 3*I*) and NTE (Fig. 3*J*) in hippocampal neurons showed colocalization of NTE with calnexin (Fig. 3*K*). Overall, these results demonstrate that NTE is associated with the ER of hippocampal neurons.

To determine the functional consequence of the loss of NTE function from the neuronal ER, we carried out further EM analysis. At 4 months, hippocampal neurons from Nes-cre:$NTE^{fl/fl}$ mice contained well preserved nuclei, but the cytoplasm displayed focal swelling and clear areas between the nucleus and plasma membrane (Fig. 4*A*). No signs of inflammation or abnormal extracellular matrix deposition were observed. In these clear regions, normal organelles were replaced by extensive smooth, folded membranes (Fig. 4*A*). By comparison, a homogenous distribution of cytoplasm and ER was observed in neurons from $NTE^{fl/fl}$ mice (Figs. 4*B*, 2*E*, and 3*D*). Vacuolated areas in cell bodies and dendrites showed flattened and sharply angulated membranes (Fig. 4 *C* and *D*). In addition, abnormal aggregates form within neuronal processes (Fig. 4*E*). These aggregates displayed branching networks of 25- to 30-nm tubules within dendrites (Fig. 4 *F* and *G*). In addition to reticular aggregates, we observed stacks of membranes and bilayers within dendrites (Fig. 4*H*). Analysis of the myelin structure of the hippocampus at the light microscope level did not reveal any gross myelin abnormalities (data not shown). EM analysis at the alveus revealed normal myelin surrounding axons (Fig. 4*I*), but in some cases, the axoplasm was displaced by large vacuoles (Fig. 4*I*, arrows). Interestingly, no apoptotic or inflammatory cells were observed around the damaged cells in the Nes-cre:$NTE^{fl/fl}$ mice. The nuclei of affected neurons did not display any evidence of shrinkage or features indicative of apoptosis.

Loss of Purkinje Cells and Behavioral Deficits. These results indicate that deletion of NTE in neuronal cells caused dramatic alterations of the ER, along with abnormal reticular aggregates and vacuolation. NTE expression in the brain is not localized to a particular brain area, but is confined to large neurons (9) with rapid protein synthesis and abundant rough ER. In addition, OP toxicity primarily affects large axons, and many sites of NTE-induced neuropathology are confined to large neurons with high metabolic activity (13).

To test whether NTE has additional consequences in other brain regions, cerebellar Purkinje cells, a population of large neurons that displays prominent expression of NTE (4, 9), were studied. Silver staining of the cerebellum and immunostaining for calbindin, a Purkinje cell-specific marker, showed a partial loss of Purkinje cells as well as thinner Purkinje dendritic trees in the molecular layer of the Nes-cre:$NTE^{fl/fl}$ cerebellum (Fig. 5 *B* and *D*). Purkinje cell loss was observed as early as 4 weeks of age. In contrast, Purkinje cells (Fig. 5 *A* and *C*) and the granule cells of the $NTE^{fl/fl}$ controls were morphologically normal (Fig. 5*A*). Immunostaining using an antibody against the neuronal marker MAP-2 confirmed the decrease of Purkinje dendritic trees in the molecular layer of the cerebellum of Nes-cre:$NTE^{fl/fl}$ (Fig. 5*F*), whereas $NTE^{fl/fl}$ appear normal (Fig. 5*E*). Neurons in the molecular layer appear normal in both groups (Fig. 5 *E* and *F*).

These observations suggest that cerebellar functions may be compromised by the loss of NTE. To evaluate dysfunctions in the Nes-cre:$NTE^{fl/fl}$ mice, we tested their performance on a rotarod behavioral test. Rotarod test performed at 1 month of age revealed no difference between Nes-cre:$NTE^{fl/fl}$ mice and $NTE^{fl/fl}$ controls (Fig. 5*G*). By contrast, although $NTE^{fl/fl}$ control mice (6 months) stay on the rotarod for 300 s after training, Nes-cre:$NTE^{fl/fl}$ mice remain for 142.3 ± 18.2 s, showing a significant decrease in their motor ability (Fig. 5*H*). Both $NTE^{fl/fl}$ controls and Nes-cre:$NTE^{fl/fl}$ mice improved during the three training sessions (Fig. 5*H*). Although no ataxia or paralysis has

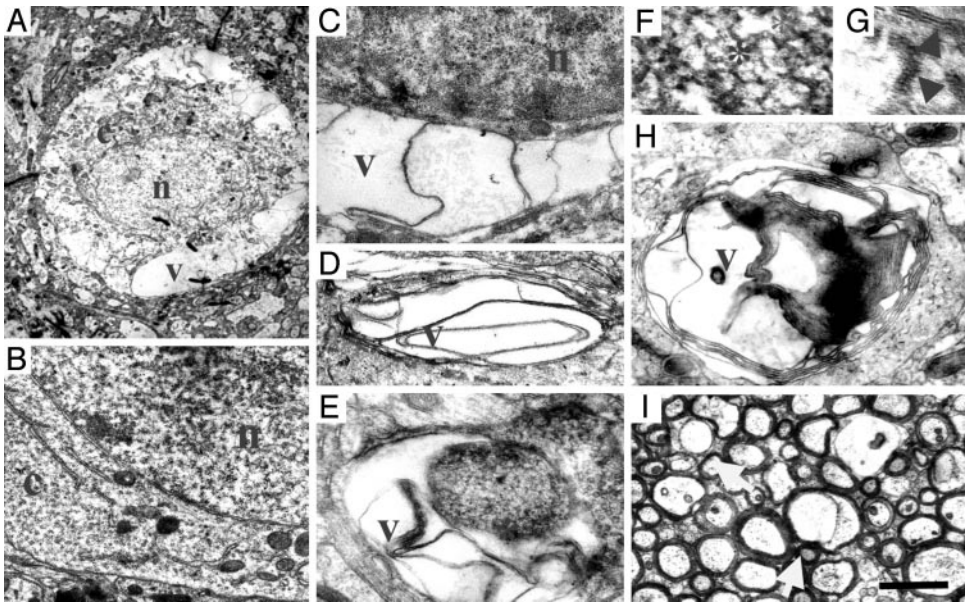

Fig. 4. Intracytoplasmic vacuolation, reticular aggregates and ER abnormalities. (*A*) A neuronal cell body from a 4.5-month-old Nes-cre:$NTE^{fl/fl}$ with normal nucleus (n) surrounded by cytoplasm (c), which in multiple areas appears swollen and clear or has been replaced by vacuoles (v) extending from the nucleus to the plasma membrane. (*B*) Neuron from a 4.5-month-old $NTE^{fl/fl}$ control mouse showing granular ER, many free ribosomes, mitochondria, and Golgi apparatus filling the cytoplasm (c) between the nucleolus (n) and the plasma membrane. Surrounding neuropil contains normal axonal and dendritic processes. Vacuolated cell body (*C*) and dendritic process (*D*) in Nes-cre:$NTE^{fl/fl}$ showing flattened and sharply angulated membranes. (*E*) A vacuolated process in the neuropil of Nes-cre:$NTE^{fl/fl}$ mouse filled with abnormal aggregates and smooth membranes. (*F*) Aggregates display a branching reticular appearance and form tubular networks and angular rods within the dendrites. (*G*) Pentalaminar structures (arrows) form the branched network in the dendrites of Nes-cre:$NTE^{fl/fl}$ mice. (*H*) Large abnormal process within the neuropil of Nes-cre:$NTE^{fl/fl}$ mice containing reticular and vacuolar inclusions with multilayered membranes. (*I*) Normal myelin surrounding nerve fibers at the alveus of the hippocampus of Nes-cre:$NTE^{fl/fl}$ mouse. In some cases, myelin sheaths enclose a clear vacuole which displaces the axoplasm to the periphery (arrows). (Scale bar, 1.4 μm in *A*; 1 μm in *B–D* and *H*; 0.4 μm in *E*; 0.2 μm in *F*; 0.1 μm in *G*; and 1.5 μm in *I*.)

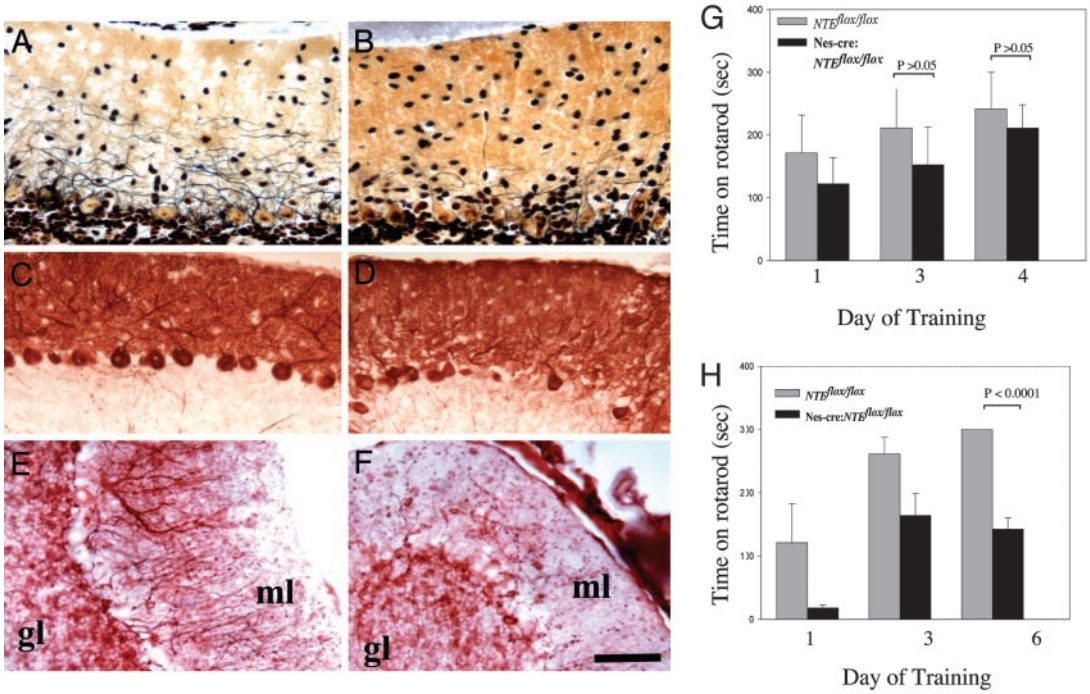

Fig. 5. Loss of Purkinje cells and behavioral deficits caused by brain deletion of NTE. (*A*) Normal Purkinje cell appearance and Purkinje dendritic tree extension revealed by silver staining in the molecular layer of the cerebellum of $NTE^{fl/fl}$ mice. (*B*) Loss of Purkinje trees and reduced dendritic tree extension and complexity by silver stain of the cerebellum of Nes-cre:$NTE^{fl/fl}$ mice. (*C*) Normal number of calbindin positive Purkinje cells in $NTE^{fl/fl}$ mice. (*D*) Loss of calbindin positive Purkinje cells from Nes-cre:$NTE^{fl/fl}$. (*E*) Normal appearance of MAP-2 positive Purkinje cell dendrites and neurons in the molecular layer of $NTE^{fl/fl}$ mice. (*F*) Loss of MAP-2 positive dendritic trees in the cerebellum. (*G*) No behavioral differences observed at a rotarod behavioral test measuring motor coordination between 4-week-old $NTE^{fl/fl}$ ($n = 4$) and Nes-cre:$NTE^{fl/fl}$ mice ($n = 5$), $P > 0.05$. (*H*) Evident coordination defects of 5-month-old Nes-cre:$NTE^{fl/fl}$ mice ($n = 4$), when compared to $NTE^{fl/fl}$ littermate controls ($n = 7$), $P < 0.0001$. GL, granular layer. (Scale bar, 50 μm.)

been observed to date, these results suggest that loss of NTE in the brain can contribute to behavioral defects.

Discussion

Conditional inactivation of the mouse NTE gene resulted in elimination of NTE protein in the central nervous system. Loss of NTE function caused degeneration of large neurons accompanied by the formation of intracellular vacuoles and abnormal reticular aggregates within cell bodies. A conspicuous feature of cells lacking NTE is the swelling of the neuronal cytoplasm, disruption and loss of ER membranes, and creation of large vacuoles reminiscent of the *Drosophila sws* phenotype (2).

NTE/*sws* represents a transmembrane protein containing a region similar to the regulatory subunit of cAMP-binding proteins and a catalytic serine esterase that are well conserved in yeast, *Caenorhabditis elegans*, *Drosophila*, and human (1, 2). The high degree of evolutionary conservation, together with the remarkably specific and pervasive intracellular neuronal deficits caused by a loss of function, indicates that NTE/*sws* is required for several fundamental biological processes. Loss of function of *Drosophila sws* is thought to be involved in axonal–glial cell interactions in the fly brain. Mutations in *sws* produce excessive wrapping of neurons by glial cells and brain vacuolation associated with glial hyperwrapping (2). The vacuolar pathology caused by loss of NTE in mice appears to be primarily in neurons, but potential effects on glia are not excluded. It is striking that the same vacuolar defects are observed in the *Drosophila sws* mutants and the conditional NTE mice. This substantiates the evolutionary conservation of function for this essential gene.

Modification of NTE by OP compounds leads to neuropathy in humans (14). Classic OP-induced delayed neuropathy has not been observed in mice (13). NTE heterozygote mice ($NTE^{+/-}$) show 40% decrease in esterase activity and do not develop neurodegeneration (4). By contrast, Nes-cre:$NTE^{fl/fl}$ mice show a 90% decrease in NTE activity, which leads to neurodegeneration. Future analysis will be needed to determine the consequences of this degeneration and the behavioral patterns of the Nes-cre:$NTE^{fl/fl}$ mice, as well as their response to OPs.

Nes-cre:$NTE^{fl/fl}$ mice develop neurodegeneration characterized by accumulation of intracellular aggregates and cytoplasmic vacuolation. The biochemical basis for NTE in neurodegeneration is unknown. It has been postulated that NTE possesses phospholipase (15) and lysophospholipase activity (16), in addition to its ability to hydrolyze carboxy ester substrates (1). These activities suggest a role for NTE in the proper sorting of phospholipids and modification of proteins associated with membranes. Lipids within intracellular organelles are directly involved in protein sorting and membrane transport (17). In this study, we find that a grossly abnormal breakdown of organelles occurs in the cytoplasm of Nes-cre:$NTE^{fl/fl}$ hippocampal neurons resulting in conspicuous vacuolation resembling spongioform encephalopathy (18). Because NTE is closely associated with the ER and results in cellular damage when it is absent from neurons, it is plausible that abnormalities in protein folding, transport, and degradation are directly influenced by NTE perturbation. Given the broad spectrum of neurological diseases that are associated with ER dysfunction and protein aggregation, such as Alzheimer's disease and prion-induced encephalopathy, loss of function of NTE may represent a unique mechanism that contributes to neurodegenerative disease.

Note Added in Proof. While this manuscript was under review, Moser *et al*. (19) reported that embryonic lethality of NTE was due to placental failure and impaired vaculogenesis, suggesting that loss of NTE expression by neurons did not contribute to embryonic lethality.

We thank Rolf Schiff, Andrew Maleson, Tal Nuriel, and Shoana Willis for assistance; Wen-Biao Gan and his laboratory for confocal imaging advice; and Palmer Taylor, Todd Talley, Zoran Radic, Joan Heller Brown, and Amy L. Howes for experimental advice. This work was supported by National Institutes of Health Grants MH59904 (to M.V.C.) and NS37475 (to J.R.), National MS Society Grants RG2539 (to J.R.) and RG3370 (to K.A.), and awards from the Wadsworth Foundation and the National Multiple Sclerosis Society (to K.A.).

1. Lush, M. J., Li, Y., Read, D. J., Willis, A. C. & Glynn, P. (1998) *Biochem. J.* **332,** 1–4.
2. Kretzschmar, D., Hasan, G., Sharma, S., Heisenberg, M. & Benzer, S. (1997) *J. Neurosci.* **17,** 7425–7432.
3. Glynn, P. (2000) *Prog. Neurobiol.* **61,** 61–74.
4. Winrow, C. J., Hemming, M. L., Allen, D. M., Quistad, G. B., Casida, J. E. & Barlow, C. (2003) *Nat. Genet.* **33,** 477–485.
5. Johnson, M. K. (1969) *Biochem. J.* **114,** 711–717.
6. Johnson, M. K. (1970) *Biochem. J.* **120,** 523–531.
7. Akassoglou, K., Bauer, J., Kassiotis, G., Pasparakis, M., Lassmann, H., Kollias, G. & Probert, L. (1998) *Am. J. Pathol.* **153,** 801–813.
8. Kim, A. H., Yano, H., Cho, H., Meyer, D., Monks, B., Margolis, B., Birnbaum, M. J. & Chao, M. V. (2002) *Neuron* **35,** 697–709.
9. Glynn, P., Holton, J. L., Nolan, C. C., Read, D. J., Brown, L., Hubbard, A. & Cavanagh, J. B. (1998) *Neuroscience* **83,** 295–302.
10. Moser, M., Stempfl, T., Li, Y., Glynn, P., Buttner, R. & Kretzschmar, D. (2000) *Mech. Dev.* **90,** 279–282.
11. Tronche, F., Kellendonk, C., Kretz, O., Gass, P., Anlag, K., Orban, P. C., Bock, R., Klein, R. & Schutz, G. (1999) *Nat. Genet.* **23,** 99–103.
12. Li, Y., Dinsdale, D. & Glynn, P. (2003) *J. Biol. Chem.* **278,** 8820–8825.
13. Glynn, P. (1999) *Biochem. J.* **344,** 625–631.
14. Johnson, M. K. & Glynn, P. (1995) *Toxicol. Lett.* **82–83,** 459–463.
15. van Tienhoven, M., Atkins, J., Li, Y. & Glynn, P. (2002) *J. Biol. Chem.* **277,** 20942–20948.
16. Quistad, G. B., Barlow, C., Winrow, C. J., Sparks, S. E. & Casida, J. E. (2003) *Proc. Natl. Acad. Sci. USA* **100,** 7983–7987.
17. Gruenberg, J. (2001) *Nat. Rev. Mol. Cell. Biol.* **2,** 721–730.
18. Libersky, P. P., Yanagihara, R., Gibbs, C. J. & Gajdusek, D. C. (1988) *Intervirology* **29,** 115–119.
19. Moser, M., Li, Y., Vaupel, K., Kretzschmar, D., Kluge, R., Glynn, P. & Buettner, R. (2004) *Mol. Cell. Biol.* **24,** 1667–1679.